Supporting Information

Catalytic Olefin Hydrosilations Mediated by Ruthenium η^3-H_2Si σ-Complexes of Primary and Secondary Silanes

Mark C. Lipke,[1,‡] Marie-Noelle Poradowski,[2,$] Christophe Raynaud,[2]

Odile Eisenstein,*[,2] T. Don Tilley*[,1]

1. Department of Chemistry, University of California, Berkeley, Berkeley, California, 94720-1460, United States.

2. Institut Charles Gerhardt, UMR 5253 CNRS-UM-ENSCM, Université de Montpellier, cc 1501 Place E. Bataillon, 34095 Montpellier, France

‡ Present address: Department of Chemistry and Chemical Biology, Rutgers, The State University of New Jersey, New Brunswick, New Jersey 08903, United States.

$ Present address: Université Lyon 1, CNRS UMR 5246, Institut de Chimie et Biochimie Moléculaires et Supramoléculaires, 43 Boulevard du 11 Novembre 1918, F-69622 Villeurbanne, France

Corresponding Author's Email: tdtilley@berkeley.edu, odile.eisenstein@umontpellier.fr

Contents:

NMR data for 1f

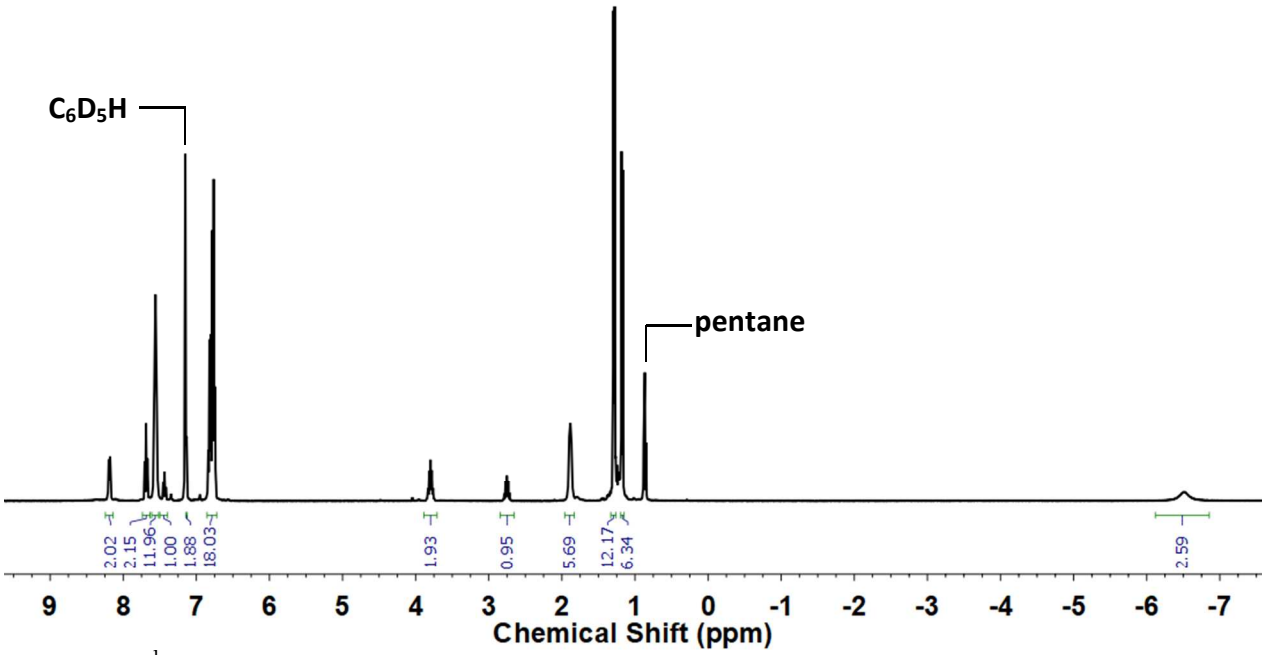

Figure S1. ^{1}H NMR spectrum (400 MHz) of **1f** in C_6D_6. Note that the aromatic C—H bonds of the Trip group overlap partially with the C—H resonance of solvent residual proteo signal.

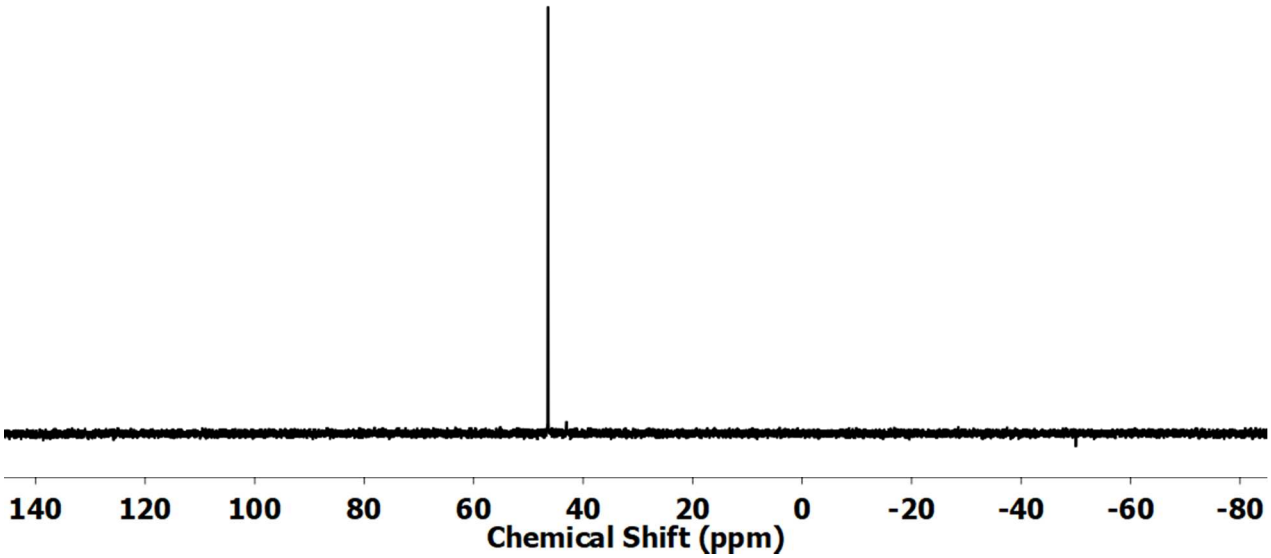

Figure S2. ^{31}P NMR spectrum (161.976 MHz) of **1f** in C_6D_6.

NMR data for 1d generated *in situ* in hydrosilation reaction mixtures

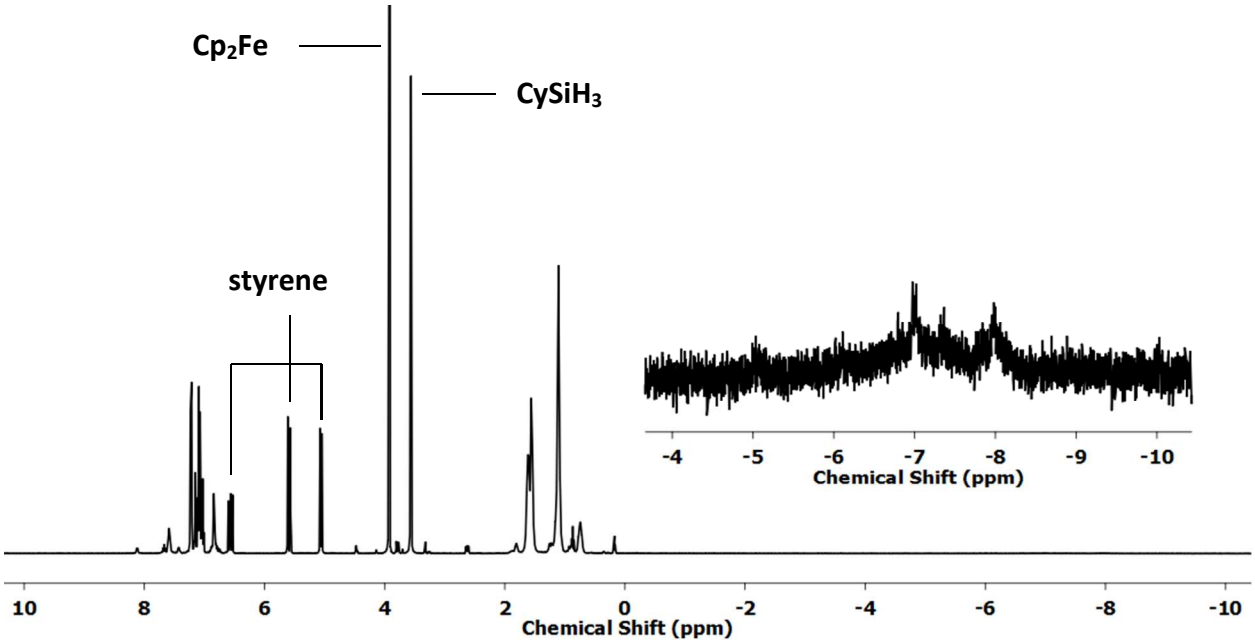

Figure S3. ^{1}H NMR spectrum (400 MHz) of hydrosilation reaction mixture immediately after mixing $CySiH_3$, styrene, and 5 mol % of **1b** in C_6D_6. Selected resonances of the alkene and silane substrate are labeled. The inset displays the broad Ru—H resonance(s) observed upon formation of **1d**.

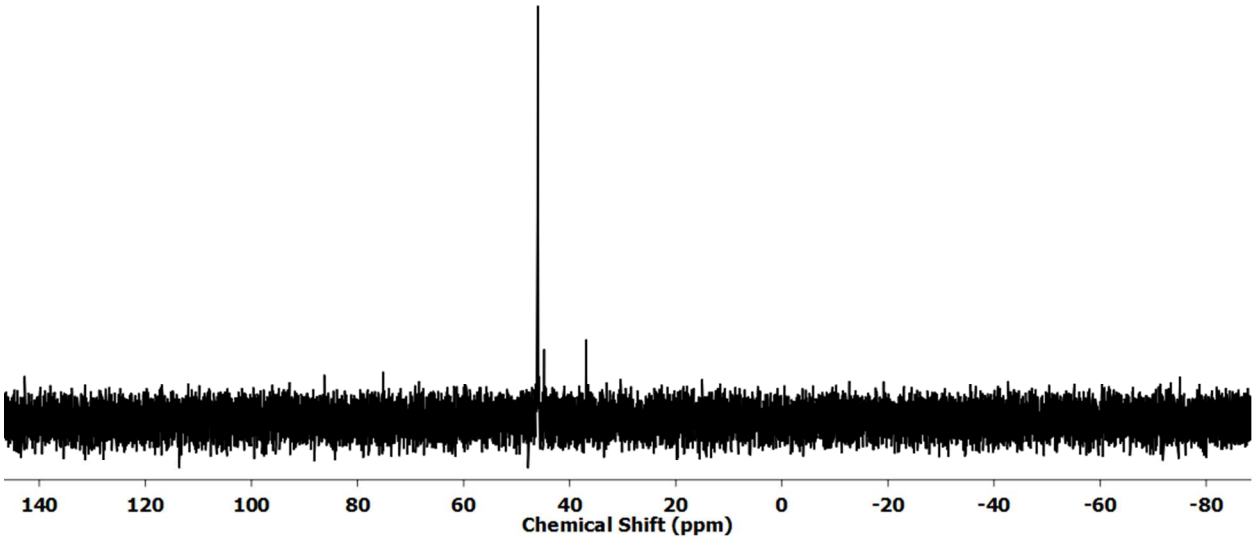

Figure S4. $^{31}P\{^{1}H\}$ NMR spectrum (161.976 MHz) of **1d** (δ 46 ppm) formed *in situ* from **1b** and excess $CySiH_3$ in the hydrosilation reaction mixture.

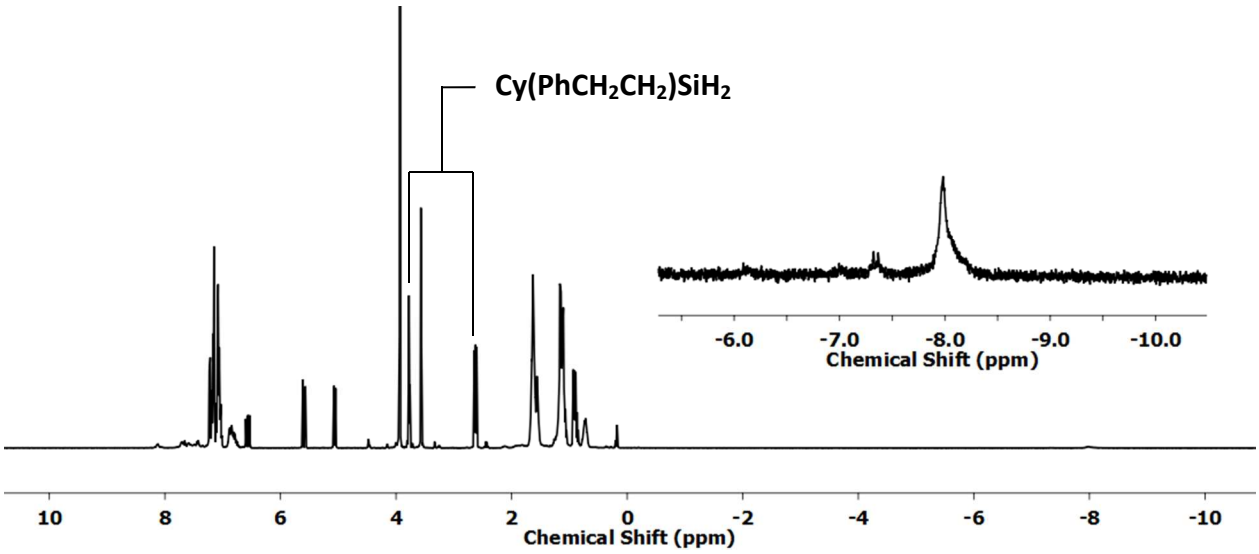

Figure S5. ^{1}H NMR spectrum (400 MHz) of hydrosilation reaction mixture 16 h after mixing $CySiH_3$, styrene, and 5 mol % of **1b** in C_6D_6. Selected resonances of the hydrosilation product are labelled. The inset shows that a new Ru—H resonance has grown in at -8.0 ppm.

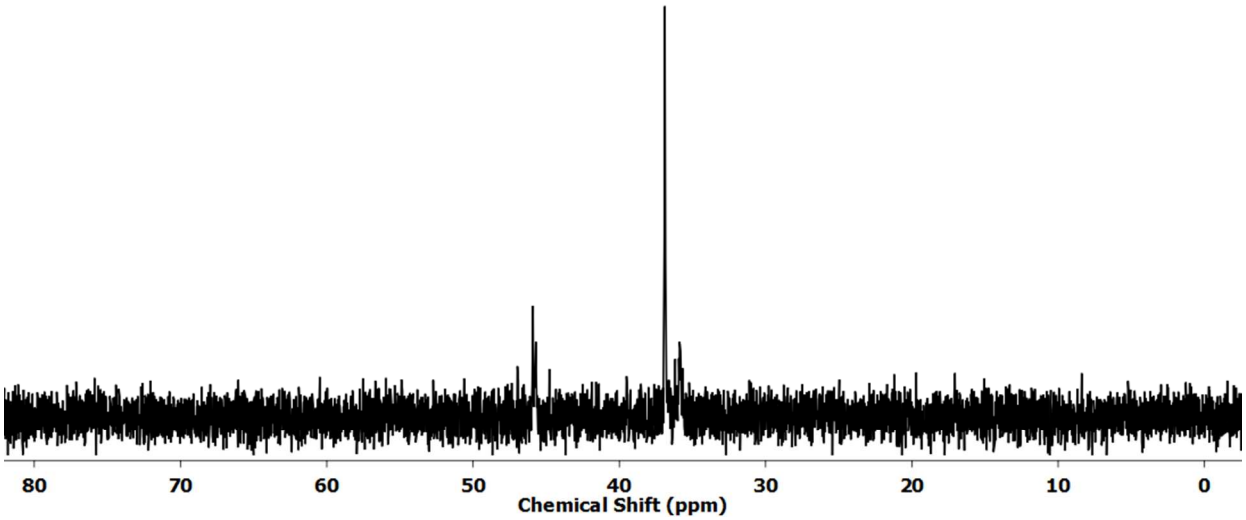

Figure S6. ^{31}P{^{1}H} NMR spectrum (161.976 MHz) of hydrosilation reaction mixture 16 h after start of the reaction. The resonance attributed to **1d** (δ 46 ppm) has mostly disappeared while new resonances can be observed between 30 – 40 ppm.

Computational Details

The calculations were carried out with the full [$PhBP^{Ph}_3$]Ru(H_3SiCy), Cy = Cyclohexyl, complex and allyl chloride was selected as a model for the alkene substrate. Localization of the extrema with the full Ru(II) complex were facilitated by an initial exploration of the potential energy surface with a simpler model in which all the aryl groups were replaced by hydrogen, and the silane and alkene were SiH_4 and ethane, respectively. DFT calculations were carried out with PBE0 hybrid functional,[1] corrected for dispersion as proposed by Grimme (D3 correction, BJ damping).[2] Calculations were performed with the Gaussian 09 suite of programs,[3] locally modified to take into account dispersion corrections for energies and their first and second derivatives. Geometry optimizations were performed without any symmetry constraints using the Def2-SVP basis set (BS1)[4] for all atoms and quasi-relativistic effective core potentials for Ru.[5] The nature of the stationary points as minima or transition states was characterized by analytical Hessian calculations. The connection between transition states, reactants, and products was verified by IRC calculations. Statistical mechanics calculations of thermal and entropic effects were carried out using the rigid rotor/harmonic oscillator approximations at 298 K and 1 atm ($G^{\text{gas,PBE0-D3bj,BS1}}$). Electronic energies were refined with single point energy calculations using the Def2-TZVPP basis set (BS2)[4] for all atoms; solvent effects (benzene) were included by means of SMD[6] single point energy calculations. Finally, Gibbs free energies in solution were estimated as:

$$G^{\text{benzene,PBE0-D3bj,BS2}} = E^{\text{benzene,PBE0-D3bj,BS2}} + G^{\text{gas,PBE0-D3bj,BS1}} - E^{\text{gas,PBE0-D3bj,BS1}}$$

NBO analyses were performed with NBO 6.0.[7]

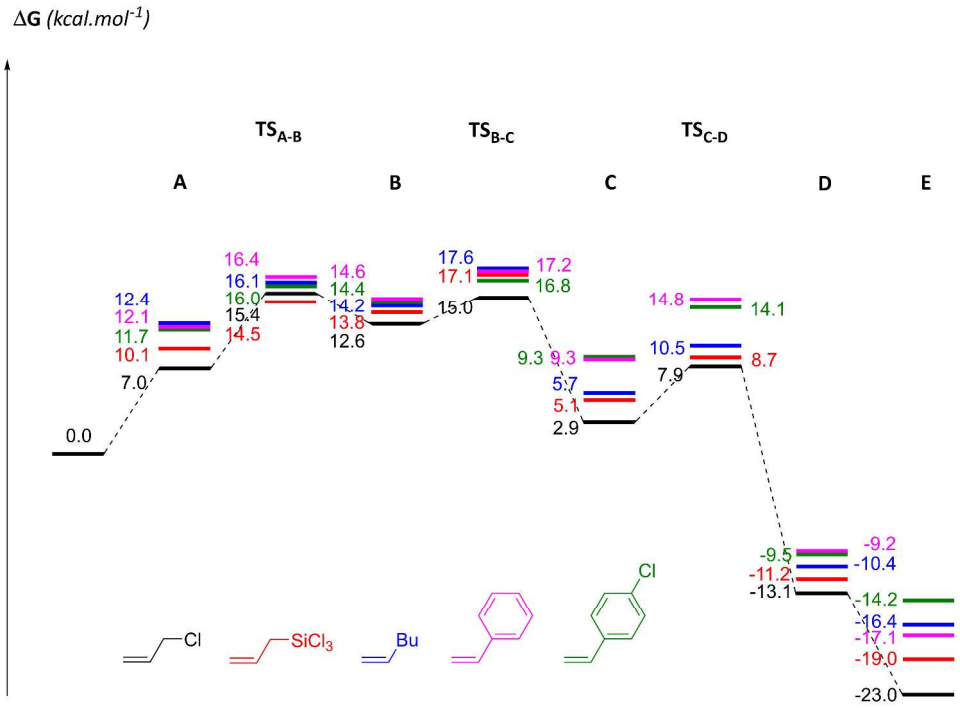

Figure S7. Gibbs Energies (kcal mol^{-1}), characterized by DFT relative to the individual complex **1d-DFT** and olefin, of intermediates and transition states for the hydrosilylation pathway involving insertion of the olefin into the terminal Ru-H bond of the catalyst.

1d-DFT + olefin	0.0	0.0	0.0	0.0	0.0
A	7.0	10.1	12.4	12.1	11.7
TS_{A-B}	15.4	14.5	16.1	16.4	16.0
B	12.6	13.8	14.2	14.6	14.4
TS_{B-C}	15.0	17.1	17.6	17.2	16.8
C	2.9	5.1	5.7	9.3	9.3
TS_{C-D}	7.9	8.7	10.5	14.8	14.1
D	-13.1	-11.2	-10.4	-9.2	-9.5
E	-23.0	-19.0	-16.4	-17.1	-14.2
A'	8.9	10.0	8.2	8.2	8.8
$TS_{A'-E}$	20.8	22.7	18.2	20.3	20.6
$TS_{A'-D'}$	26.3	23.6	22.4	22.1	21.8
D'	-7.7	-6.5	-6.2	-3.5	-3.8

Table S1. Values ((kcal mol^{-1}) corresponding to Figure S7.

Results of NBO Analysis

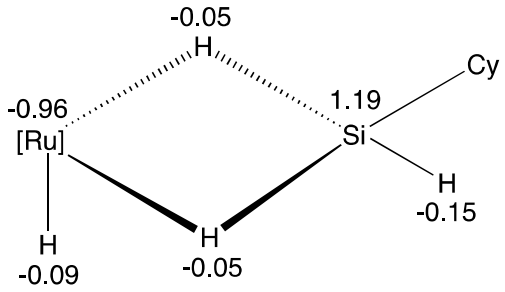

Figure S8. NBO charges in **1d-DFT**.

The Transition states are analyzed using two parameters extracted from NBO Analysis:

1° The interaction energies obtained from a second order perturbation analysis. The energies obtained through these analysis are very large since they are not compensated by electron-electron repulsion. Only relative energies should be considered. This method gives exaggerated values and even exaggerated differences.

2° The NLMO are expressed in terms of combinations of NBO. This method describes how an NBO is delocalized with other NBO to give an NLMO which contains 2 e^-. This method gives reliable information on the interaction between occupied and empty orbitals. However, coefficients associated with different olefins are similar. It is more difficult to detect differences with this representation.

Combining the two above criteria gives a rationale of why the insertion of the olefin occurs preferably in the Ru-H bond than in the Si-H bond: the Hydride on Ru is a better donor and Ru a better acceptor.

Allyl Chloride

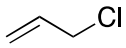

TS_{A-B} (insertion in Ru-H bond)
Total non-Lewis 13.28730 (2.605% of 510)

Second order perturbation (energy in kcal mol^{-1})

# orbital Donor	# orbital Acceptor	Energy
88. LP (1) H 20	243. BD*(1) P 1-Ru 19	231.43
88. LP (1) H 20	267. BD*(2) C 14- C 17	482.14
117. BD (2) C 14- C 17	243. BD*(1) P 1-Ru 19	24.13
117. BD (2) C 14- C 17	247. BD*(1) P 2-Ru 19	88.61
117. BD (2) C 14- C 17	251. BD*(1) P 3-Ru 19	13.19

NLMO
88. LP (1) H 20 + (243. P 1-Ru19* 0.5190) + (267. C14- C17* 0.4734)
117. BD (2) C 14- C 17 + (243. P 1-Ru19* -0.0841) + (247. P 2-Ru19* 0.4122) + (251. P 3-Ru19* -0.0753)

$TS_{A'-E}$ (Insertion in the terminal Si-H bond)
Total non-Lewis 14.14055 (2.773% of 510)

Second order perturbation (energy in kcal mol^{-1})

# orbital Donor	# orbital Acceptor	Energy
122. BD (1)Si 23- H 24	269. BD*(2) C 18- C 21	56.28
119. BD (2) C 18- C 21	245. BD*(1) H 3-Si 23	112.42

NLMO
BD (1)Si 23- H 24 + (269. C18- C21* 0.3967)
BD (2) C 18- C 21 + (245. H 3-Si23* 0.3406)

AllylSiCl3

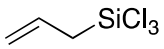

TS_{A-B} (insertion into Ru-H bond)
Total non-Lewis 13.95505 (2.501% of 558)

Second order perturbation (energy in kcal mol^{-1})

# orbital Donor	# orbital Acceptor	Energy
103. LP (1) H 20	267. BD*(1) P 1-Ru 19	234.35
103. LP (1) H 20	291. BD*(2) C 14- C 17	601.17
138. BD (2) C 14- C 17	267. BD*(1) P 1-Ru 19	21.93
138. BD (2) C 14- C 17	271. BD*(1) P 2-Ru 19	84.64
138. BD (2) C 14- C 17	275. BD*(1) P 3-Ru 19	12.34

NLMO
LP (1) H 20 + (267. P 1-Ru19* 0.5218) + (291. C14- C17* 0.4718)
BD (2) C 14- C 17 + (267. P 1-Ru19* -0.0830) + (271. P 2-Ru19* 0.4068) + (275. P 3-Ru19* -0.0768)

$TS_{A'-E}$ (insertion into terminal Si-H bond)
Total non-Lewis 15.37813 (2.756% of 558)

Second order perturbation (energy in kcal mol^{-1})

# orbital Donor	# orbital Acceptor	Energy
144. BD (1)Si 23- H 24	294. BD*(2) C 18- C 21	58.74
141. BD (2) C 18- C 21	270. BD*(1) H 3-Si 23	120.30

NLMO
BD (1)Si 23- H 24 + (294. C18- C21* 0.4041)
BD (2) C 18- C 21 + (270. H 3-Si23* 0.3475)

Hexene

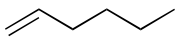

TS_{A-B} (insertion into Ru-H bond)
Total non-Lewis 13.50885 (2.608% of 518)

Second order perturbation (energy in kcal mol^{-1})

# orbital Donor	# orbital Acceptor	Energy
86. LP (1) H 20	247. BD*(1) P 1-Ru 19	242.11
86. LP (1) H 20	271. BD*(2) C 14- C 17	444.64
112. BD (2) C 14- C 17	247. BD*(1) P 1-Ru 19	22.39
112. BD (2) C 14- C 17	251. BD*(1) P 2-Ru 19	85.96

112. BD (2) C 14- C 17	255. BD*(1) P 3-Ru 19	12.65

NLMO
LP (1) H 20 + (247. P 1-Ru19* 0.5303) + (271. C14- C17* 0.4562)
BD (2) C 14- C 17 + (247. P 1-Ru19* -0.0809) + (251. P 2-Ru19* 0.4129) + (255. P 3-Ru19* -0.0787)

$TS_{A'-E}$ (Insertion into the Si-H bond)
Total non-Lewis 14.92271 (2.881% of 518)

Second order perturbation (energy in kcal mol^{-1})

# orbital Donor	# orbital Acceptor	Energy
118. BD (1)Si 23- H 24	274. BD*(2) C 18- C 21	58.43
115. BD (2) C 18- C 21	250. BD*(1) H 3-Si 23	129.70

NLMO
BD (1)Si 23- H 24 + (274. C18- C21* 0.3990)
BD (2) C 18- C 21 + (250. H 3-Si23* 0.3567)

Styrene

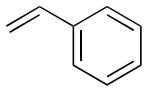

TS_{A-B} (insertion in the Ru-H bond)
Total non-Lewis 14.43963 (2.745% of 526)

Second order perturbation (energy in kcal mol^{-1})

# orbital Donor	# orbital Acceptor	Energy
88. LP (1) H 19	275. BD*(2) C 14- C 17	429.22
88. LP (1) H 19	251. BD*(1) P 1-Ru 18	233.36
114. BD (2) C 14- C 17	251. BD*(1) P 1-Ru 18	23.27
114. BD (2) C 14- C 17	255. BD*(1) P 2-Ru 18	82.26
114. BD (2) C 14- C 17	259. BD*(1) P 3-Ru 18	11.38

NLMO
LP (1) H 19 + (275. C14- C17* 0.4656) + (251. P 1-Ru18* 0.5155)
BD (2) C 14- C 17 + (251. P 1-Ru18* 0.0094 -0.0778) + (255. P 2-Ru18* 0.0161 0.4082) + (259. P 3-Ru18* -0.0083 -0.0752)

$TS_{A'-E}$ (insertion in the Si-H bond)
Total non-Lewis 15.45029 (2.937% of 526)

Second order perturbation (energy in kcal mol^{-1})

# orbital Donor	# orbital Acceptor	Energy
119. BD (1)Si 23- H 24	277. BD*(2) C 18- C 21	62.22
116. BD (2) C 18- C 21	253. BD*(1) H 3-Si 23	135.34

NLMO
BD (1)Si 23- H 24 + (277. C18- C21* -0.4178)
BD (2) C 18- C 21 + (253. H 3-Si23* 0.3584)

***p*-Chlorostyrene**

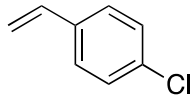

TS_{A-B} (insertion in the Ru-H bond)
Total non-Lewis 14.55553 (2.686% of 542)

Second order perturbation (energy in kcal mol^{-1})

# orbital Donor	# orbital Acceptor	Energy
93. LP (1) H 19	283. BD*(2) C 14- C 17	444.18
93. LP (1) H 19	259. BD*(1) P 1-Ru 18	231.96
122. BD (2) C 14- C 17	259. BD*(1) P 1-Ru 18	23.34
122. BD (2) C 14- C 17	263. BD*(1) P 2-Ru 18	82.23
122. BD (2) C 14- C 17	267. BD*(1) P 3-Ru 18	11.35

NLMO
LP (1) H 19 + (283. C14- C17* 0.4690) + (259. P 1-Ru18* 0.5131)
BD (2) C 14- C 17 + (259. P 1-Ru18* 0.0098 -0.0777) + (263. P 2-Ru18* 0.0162 0.4074)+ (267. P 3-Ru18* -0.0084 -0.0751)

$TS_{A'-E}$ (insertion into SiH)
Total non-Lewis 16.24545 (2.997% of 542)

Second order perturbation (energy in kcal mol^{-1})

# orbital Donor	# orbital Acceptor	Energy
128. BD (1)Si 23- H 24	286. BD*(2) C 18- C 21	62.95
125. BD (2) C 18- C 21	262. BD*(1) H 3-Si 23	134.31

NLMO
BD (1)Si 23- H 24 + (286. C18- C21* -0.4197)
BD (2) C 18- C 21 + (262. H 3-Si23* 0.3576)

References

1. Adamo, C.; Barone, V. Toward Reliable Density Functional Methods without Adjustable Parameters: The PBE0 Model. *J. Chem. Phys.* **1999**, *110*, 6158−6170.
2. (a) Grimme, S.; Antony, J.; Ehrlich, S.; Krieg, H. A Consistent and Accurate Ab Initio Parametrization of Density Functional Dispersion Correction (DFT-D) for the 94 Elements H – Pu. *J. Chem. Phys.* **2010**, *132*, 154104. (b) Grimme, S.; Ehrlich, S.; Goerigk, L. Effect of

the Damping Function in Dispersion Corrected Density Functional Theory. *J. Comput. Chem.* **2011**, *32*, 1456−1465.

3. Frisch, M. J.; Trucks, G. W.; Schlegel, H. B.; Scuseria, G. E.; Robb, M. A.; Cheeseman, J. R.; Scalmani, G.; Barone, V.; Mennucci, B.; Petersson, G. A.; Nakatsuji, H.; Caricato, M.; Li, X.; Hratchian, H.P.; Izmaylov, A. F.; Bloino, J.; Zheng, G.; Sonnenberg, J. L.; Hada, M.; Ehara, M.; Toyota, K.; Fukuda, R.; Hasegawa, J.; Ishida, M.; Nakajima, T.; Honda, Y.; Kitao, O.; Nakai, H.; Vreven, T.; Montgomery, J. A., Jr.; Peralta, J. E.; Ogliaro, F.; Bearpark, M.; Heyd, J. J.; Brothers, E.; Kudin, K. N.; Staroverov, V. N.; Kobayashi, R.; Normand, J.; Raghavachari, K.; Rendell, A.; Burant, J. C.; Iyengar, S. S.; Tomasi, J.; Cossi, M.; Rega, N.; Millam, J. M.; Klene, M.; Knox, J. E.; Cross, J. B.; Bakken, V.; Adamo, C.; Jaramillo, J.; Gomperts, R.; Stratmann, R. E.; Yazyev, O.; Austin, A. J.; Cammi, R.; Pomelli, C.; Ochterski, J. W.; Martin, R. L.; Morokuma, K.; Zakrzewski, V. G.; Voth, G. A.; Salvador, P.; Dannenberg,J.J.; Dapprich,S.; Daniels,A.D. ;Farkas,O.; Foresman, J. B.; Ortiz, J. V.; Cioslowski, J.; Fox, D. J. *Gaussian 09*, revision B.01; Gaussian, Inc.: Wallingford, CT, 2009.
4. Weigend, F.; Ahlrichs, R. Balanced Basis Sets of Split Valence, Triple Zeta Valence and Quadruple Zeta Valence Quality for H to Rn: Design and Assessment Of Accuracy. *Phys. Chem. Chem. Phys.* **2005**, *7,* 3297−3305.
5. (a) Andrae, D.; Häussermann, U.; Dolg, M.; Stoll, H.; Preuss, H. Energy-Adjusted Ab Initio Pseudopotentials for the Second and Third Row Transition Elements. *Theor. Chim. Acta* **1990**, *77*, 123−141. (b) Metz, B.; Stoll, H.; Dolg, M. Small-Core Multiconfiguration-Dirac–Hartree–Fock-Adjusted Pseudopotentials for Post-D Main Group Elements: Application to PbH and PbO. *J. Chem. Phys.* **2000**, *113*, 2563−2569.

6. Marenich, A. V.; Cramer, C. J.; Truhlar, D. G. Universal Solvation Model Based on Solute Electron Density and on a Continuum Model of the Solvent Defined by the Bulk Dielectric Constant and Atomic Surface Tensions. *J. Phys. Chem. B* **2009**, *113*, 6378−6396.
7. Glendening, E. D.; Badenhoop, J. K.; Reed, A. E.; Carpenter, J.E.; Bohmann, J. A.; Morales, C. M.; Landis, C. R.; Weinhold, F. *NBO 6.0*; Theoretical Chemistry Institute, University of Wisconsin: Madison, WI, 2013.